Noninvasive Imaging of Early Venous Thrombosis by ^{19}F Magnetic Resonance Imaging With Targeted Perfluorocarbon Nanoemulsions

Sebastian Temme, PhD; Christoph Grapentin, PhG; Christine Quast, MD; Christoph Jacoby, PhD; Maria Grandoch, MD; Zhaoping Ding, MD; Christoph Owenier, BSc; Friederike Mayenfels, PhD; Jens W. Fischer, PhD; Rolf Schubert, PhD; Jürgen Schrader, MD*; Ulrich Flögel, PhD*

Background—Noninvasive detection of deep venous thrombi and subsequent pulmonary thromboembolism is a serious medical challenge, since both incidences are difficult to identify by conventional ultrasound techniques.

Methods and Results—Here, we report a novel technique for the sensitive and specific identification of developing thrombi using background-free ^{19}F magnetic resonance imaging, together with α2-antiplasmin peptide ($\alpha2^{AP}$)–targeted perfluorocarbon nanoemulsions (PFCs) as contrast agent, which is cross-linked to fibrin by active factor XIII. Ligand functionality was ensured by mild coupling conditions using the sterol-based postinsertion technique. Developing thrombi with a diameter <0.8 mm could be visualized unequivocally in the murine inferior vena cava as hot spots in vivo by simultaneous acquisition of anatomic matching ^{1}H and ^{19}F magnetic resonance images at 9.4 T with both excellent signal-to-noise and contrast-to-noise ratios (71±22 and 17±5, respectively). Furthermore, $\alpha2^{AP}$-PFCs could be successfully applied for the diagnosis of experimentally induced pulmonary thromboembolism. In line with the reported half-life of factor XIIIa, application of $\alpha2^{AP}$-PFCs >60 minutes after thrombus induction no longer resulted in detectable ^{19}F magnetic resonance imaging signals. Corresponding results were obtained in ex vivo generated human clots. Thus, $\alpha2^{AP}$-PFCs can visualize freshly developed thrombi that might still be susceptible to pharmacological intervention.

Conclusions—Our results demonstrate that ^{1}H/^{19}F magnetic resonance imaging, together with $\alpha2^{AP}$-PFCs, is a sensitive, noninvasive technique for the diagnosis of acute deep venous thrombi and pulmonary thromboemboli. Furthermore, ligand coupling by the sterol-based postinsertion technique represents a unique platform for the specific targeting of PFCs for in vivo ^{19}F magnetic resonance imaging. (***Circulation*. 2015;131:1405-1414. DOI: 10.1161/CIRCULATIONAHA.114.010962.)**

Key Words: fluorocarbons ■ magnetic resonance imaging ■ molecular imaging ■ pulmonary embolism ■ venous thrombosis

Thrombosis plays a crucial role in a variety of cardiovascular diseases such as myocardial infarction, deep venous thrombosis, and pulmonary embolism, which are major causes of morbidity and mortality. More recently, it has been shown that patients with tumor have up to an 7-fold and obese people a 2.5-fold increased risk of developing thromboembolic events[1,2] caused by systemically increased proinflammatory conditions and the release of prothrombotic factors. Thus, visualization and specific identification of thrombi by imaging techniques address an important clinical problem.

Clinical Perspective on p 1414

Thrombi can be visualized noninvasively by ultrasound,[3] computed tomography,[4] or magnetic resonance (MR) imaging (MRI).[5] MRI is free of ionizing radiation and has high spatial resolution in deep tissues that are not accessible by ultrasound. However, thrombus detection by conventional MRI

Received May 3, 2014; accepted February 13, 2015.

From Institut für Molekulare Kardiologie (S.T., C.Q., C.J., Z.D., C.O., J.S., U.F.), Institut für Pharmakologie und klinische Pharmakologie (M.G., J.W.F.), and Cardiovascular Research Institute Düsseldorf (J.W.F., J.S., U.F.), Heinrich-Heine-Universität Düsseldorf, Düsseldorf, Germany; Institut für Pharmazeutische Technologie und Biopharmazie, Albert-Ludwigs-Universität, Freiburg, Germany (C.G., F.M., R.S.); and Klinik für Kardiologie, Pneumologie und Angiologie, Universitätsklinikum Düsseldorf, Düsseldorf, Germany (C.Q., C.J., U.F.).

*Drs Schrader and Flögel contributed equally.

The online-only Data Supplement is available with this article at http://circ.ahajournals.org/lookup/suppl/doi:10.1161/CIRCULATIONAHA.114.010962/-/DC1.

Correspondence to Ulrich Flögel, PhD, Institut für Molekulare Kardiologie, Heinrich-Heine-Universität Düsseldorf, Postfach 101007, 40001 Düsseldorf, Germany. E-mail floegel@uni-duesseldorf.de

with ^{1}H MR angiography or T1/T2-weighted ^{1}H MRI is difficult because small, nonocclusive thrombi have only a minor impact on blood flow and may not give rise to a clear signal in weighted images. To overcome this limitation, gadolinium-based probes raised against fibrin within the thrombus have been developed (EP-2104R).[6–11] Another specific marker of developing thrombi is factor XIIIa (FXIIIa), which cross-links α2-antiplasmin with fibrin during the early phase of thrombus formation.[12,13] Probes based on α2-antiplasmin have been used for ex vivo or in vivo labeling of thrombi by near-infrared fluorescence, scintigraphy, or gadolinium-enhanced ^{1}H MRI.[14–17]

Recently, ^{19}F MRI has emerged as a promising novel technique for molecular imaging. For this, emulsified, biologically inert perfluorocarbons (perfluorocarbon nanoemulsions [PFCs]) are used as a contrast agent to follow the fate of ex vivo or in vivo PFC-labeled cells.[18–20] Because ^{19}F is physiologically found in biological tissue in only trace amounts, the resulting fluorine signal displays an excellent degree of specificity. Merging of ^{19}F images with corresponding ^{1}H data sets enables the exact anatomic localization of the ^{19}F signal. Because ^{19}F MRI generates a positive contrast as a "hot spot," it is especially useful for heterogeneous tissue in which ^{1}H-based contrast is challenged by susceptibility artifacts or sparse proton density, complicating the interpretation of effects obtained by other contrast agents. Until now, ^{19}F MRI has been used predominantly for immune cell tracking in a variety of clinically relevant inflammation models.[21–29] This approach is based on the rapid uptake of intravenously injected PFCs by circulating monocytes that subsequently migrate into the inflamed area, resulting in a local accumulation of ^{19}F-loaded immune cells.

In the present study, we report a novel procedure for the generation of targeted PFCs that makes use of a sterol-based postinsertion technique (SPIT) to generate α2-antiplasmin–labeled PFCs ($\alpha2^{AP}$-PFCs). SPIT allows modification of preformed PFCs under mild conditions that maintain the functionality of labile ligands. Using $\alpha2^{AP}$-PFCs, we were able to detect the formation of developing deep venous thrombi and pulmonary embolism with ^{1}H/^{19}F MRI in vivo with a high specificity and sensitivity.

Methods

An expanded Methods section can be found in the online-only Data Supplement.

Perfluorocarbon Nanoemulsions

PFCs were prepared as previously reported (see the online-only Data Supplement for more details).[22,23]

Sterol-Based Postinsertion Technique

Generation of the Cholesterol-PEG$_{2000}$-Maleimide Anchor

An equimolar mixture of maleimide-PEG$_{2000}$-NH$_2$ (Jenkem Technology, Plano, TX), cholesteryl chloroformate (Sigma Aldrich, Seelze, Germany), and the activator triethylamine (Carl Roth, Karlsruhe, Germany) in water-free methylene chloride was prepared. The mixture was stirred for 24 hours under exclusion of light in a nitrogen atmosphere. The resulting cholesterol-PEG$_{2000}$-maleimide was purified by chromatography with the use of a Sephadex LH-20 column and validated by ^{1}H nuclear magnetic resonance spectroscopy. Aliquots were stored at −80°C under argon.

Coupling of $\alpha2^{AP}$ to the Cholesterol-PEG Anchor

To generate PFCs for site-specific targeting of thrombi, we used a 14–amino acid peptide derived from $\alpha2^{AP}$ that is known to be cross-linked to fibrin at the glutamine Q3 by FXIIIa.[15–17] As control, Q3 was converted to alanine (Q3A), leading to a low-affinity substrate for FXIIIa.[17] Both peptides were further functionalized with a cysteine residue at amino acid position 13 (Figure I in the online-only Data Supplement) for coupling to the cholesterol-PEG anchor. For immunofluorescence studies, carboxyfluorescein was linked via an additional lysine at the c-terminal tryptophan (W14).

All peptides (Genaxxon, Ulm, Germany) were dissolved in sterile phosphate buffer (10 mmol/L phosphate isotonized with glycerol, pH 7.4) to 5 mg/mL. The peptides were added to the cholesterol-PEG$_{2000}$-maleimide anchor, and the mixture was shaken at 17°C for 20 hours at 700 rpm. The cholesterol anchor was used in 10-fold excess compared with the ligand, thus allowing a quantitative coupling of peptides. During the incubation period, the thiol group of the cysteine residue and the maleimide group form a stable thioether bond.[30] Free maleimide groups were subsequently deactivated by the addition of mercaptoethanolamine. This way, a mixture of cholesterol-PEG$_{2000}$-peptide and deactivated cholesterol-PEG$_{2000}$ (approximate ratio of 1:10) was obtained and used in the following insertion step.

Postinsertion

Preformed PFCs were incubated with the obtained mixture on a rotary shaker at 17°C for 1 hour. As illustrated in Figure 1A, this leads to the spontaneous insertion of the cholesterol moiety into the phospholipid layer of the PFC[31] (molar ratio of phospholipid to cholesterol derivative, 20:1). PEGylated but nontargeted PFCs were formed by incubation with nonmodified cholesterol-PEG$_{2000}$ only.

Characterization of PFCs

The resulting emulsions were characterized by photon correlation spectroscopy on a Malvern Zetasizer Nano ZS (Malvern Instruments, Herrenberg, Germany) to determine the hydrodynamic diameter, the polydispersity index, and the ζ potential. Compared with nonmodified PFCs, we observed a slight increase in size (diameter: nontargeted PFCs, 149±15 nm; $\alpha2^{AP}$-PFCs, 165±13 nm), a similar size distribution (polydispersity index: nontargeted PFCs, 0.14±0.01; $\alpha2^{AP}$-PFCs, 0.16±0.05), but a less negative ζ potential (nontargeted PFCs, −37.2±4 mV; $\alpha2^{AP}$-PFCs, −11.7±7 mV) for the targeted or PEGylated PFCs. This indicates the successful incorporation of chol-PEG-$\alpha2^{AP}$ into the PFC nanoparticles. ^{19}F MRI measurements confirmed that all nanoemulsions exhibited the same fluorine content (Figure IIB in the online-only Data Supplement).

Animal Experiments

Animal experiments were in accordance with institutional guidelines on animal care. Male mice (C57BL/6; body weight, 25–30 g; age, 8–10 weeks) used in this study were bred at the central animal facility of the Heinrich Heine University (Düsseldorf, Germany). They were fed a standard chow diet and received tap water ad libidum.

Induction of Venous Thrombi and Pulmonary Thromboembolism

During surgery, mice were kept under anesthesia with 1.5% isoflurane. Buprenorphin was injected for analgesia. A median laparotomy was performed, and the inferior vena cava was exposed at the anatomic level of both kidneys. Subsequently, a filter paper (1×4 mm^2) soaked with 10% $FeCl_3$ was placed on top of the vessel and incubated for 8 minutes. To ensure the location of the $FeCl_3$-soaked filter paper on top of the vessel surface, 2 stretches of parafilm were placed on both sides of the vessel. After removal of the filter paper, the vessel was washed with 0.9% NaCl to remove residual

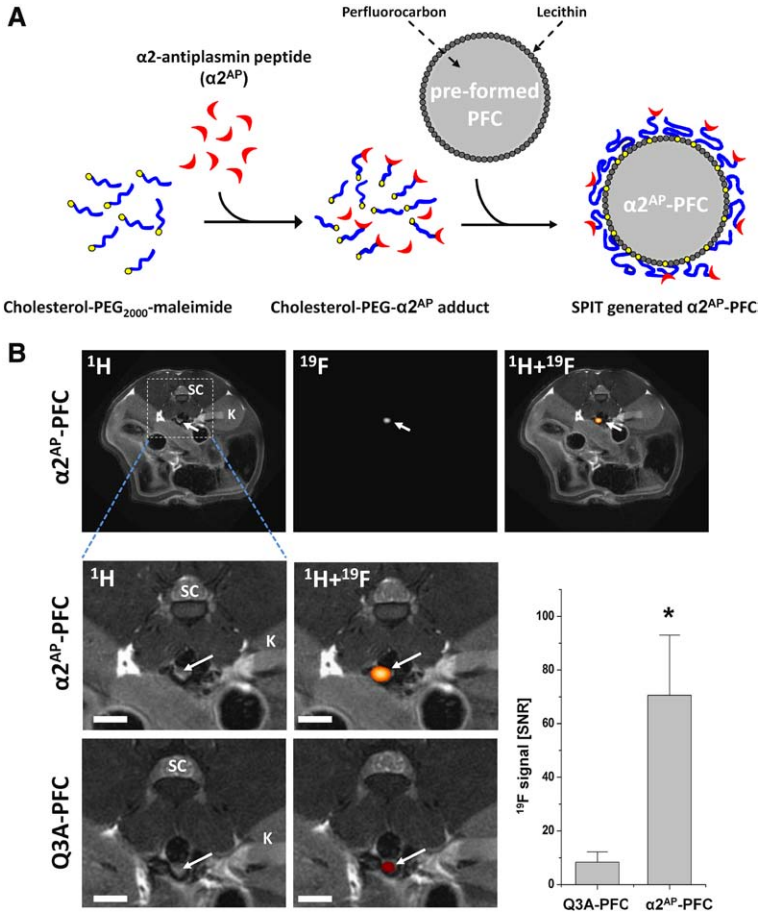

Figure 1. Specific detection of thrombus formation using sterol-based postinsertion technique (SPIT)–generated α2-antiplasmin peptide ($\alpha2^{AP}$)–perfluorocarbon nanoemulsions (PFCs). **A**, Scheme showing the principle of SPIT for the generation of $\alpha2^{AP}$-PFCs. First, $\alpha2^{AP}$ (red) is linked to a cholesterol-PEG_{2000}-maleimide (cholesterol, yellow dot; PEG, blue thread) via a stable thioether bond. The cholesterol-PEG-$\alpha2^{AP}$ adduct is then incubated with preformed PFCs, which results in a spontaneous insertion of the cholesterol moiety into the lecithin layer of the PFCs. SPIT is conducted at very mild conditions that maintain the functionality of the targeting ligand. **B**, In vivo ^{1}H and ^{19}F magnetic resonance imaging (MRI) scans after generation of a $FeCl_3$-induced thrombus (arrows) in the inferior vena cava. **Left top**, Anatomic overview of the surgery region at the level of both kidneys (K) with the back of the animal to the top. **Middle** and **Right**, The corresponding ^{19}F and the merged ^{1}H/^{19}F image, respectively. Dashed lines comprise the magnified areas shown below with ^{1}H (**left**) and merged images (**middle**; ^{19}F, red) of mice that received $\alpha2^{AP}$-PFCs (**top**) or Q3A-PFCs (**bottom**). Only injection of $\alpha2^{AP}$-PFCs resulted in strong ^{19}F signals in the area of interest. Overlay with the anatomic ^{1}H MRI clearly confirmed the location of the ^{19}F signal (red) in the thrombus, which emerges in the proton image as a dark gray semicircular structure at the ventral site of the inferior vena cava (arrows). The imaging sequence used (rapid acquisition with relaxation enhancement) results in a signal void of blood signals. Thus, the nonoccluded vessel part of the vena cava appears black. Scale bars represent 2.5 mm. Graph shows the quantification of the ^{19}F signal (signal-to-noise ratio) in thrombi from $\alpha2^{AP}$-PFC– or Q3A-PFC–treated animals. Data are mean±SD of n=6 (Q3A-PFC) and n=8 ($\alpha2^{AP}$-PFC) individual experiments (*P<0.05). SC indicates spinal cord.

$FeCl_3$. PFCs (3 mmol/kg body weight) were injected into the tail vein ≈5 minutes before thrombus induction or 5, 15, 30, 60, or 90 minutes after thrombus induction. Subsequently, MRI scans were performed at 2, 8, or 24 hours after surgery. To induce pulmonary thromboembolism, a mixture of human thrombin (Sigma-Aldrich, Seelze, Germany; 10 U/25 g body weight) and $\alpha2^{AP}$-PFCs (or unmodified PFCs/Q3A-PFCs as control) was injected that resulted in an 80% survival rate. ^{1}H/^{19}F MRI measurements were performed 24 hours later.

MRI Studies

Experiments were performed with a vertical 9.4-T Bruker AVANCE III Wide Bore nuclear magnetic resonance spectrometer (Bruker, Rheinstetten, Germany) operating at frequencies of 400.21 MHz for ^{1}H and 376.54 MHz for ^{19}F measurements using microimaging units as described previously.[22–25,27,32] Mice were anaesthetized with 1.5% isoflurane and were kept at 37°C during the measurements. Data were acquired with the use of a 25-mm birdcage resonator tunable to ^{1}H and ^{19}F. After acquisition of the morphological ^{1}H images, the resonator was tuned to ^{19}F, and anatomically matching ^{19}F images were recorded (see the online-only Data Supplement for a more detailed description of MRI setup, acquisition parameters, and quantification procedures). An overview over all imaging parameters used for ^{1}H/^{19}F MRI is given in Table I in the online-only Data Supplement.

In Vitro Thrombus Studies

Human blood was obtained by venous puncture and collected on ice. Blood (100 μL) was transferred to a round-bottom 96-well plate and incubated at 37°C for 15 minutes. Next, 25 μL PFCs (nontargeted PFCs or $\alpha2^{AP}$-PFCs) were added to each well, and the plate was further incubated for 90 minutes at 37°C under constant motion. The blood clots were extensively washed with cold PBS and subjected to ^{1}H/^{19}F MRI. Details about PFC uptake studies by murine blood are given in the expanded Method section of the online-only Data Supplement.

Cytotoxicity Assay

Murine splenocytes were obtained from C56BL/6 mice, incubated with the different PFCs, and analyzed as described in the expanded Method section of the online-only Data Supplement.

Flow Cytometry

Mice were killed by cervical dislocation, and thrombi were excised and digested in streptokinase/plasmin (150/2 U/mL) for 30 minutes at 37°C under constant shaking. To generate a single-cell suspension, thrombi were passed through a 70-μm cell strainer (BD Biosciences, Heidelberg, Germany), washed with fluorescence-activated cell sorter buffer, and stained for 30 minutes with fluorochrome-coupled antibodies as described in the online-only Data Supplement.

Histology and Fluorescence Microscopy

Excised thrombi and lungs were fixed in 4% paraformaldehyde or embedded in Tissue-Tek (Weckert Labortechnik, Kitzingen, Germany) and frozen at −20°C. Sections of 8 or 14 μm were cut and processed for immunohistochemical staining as described previously[23,24,32] (see the online-only Data Supplement for more details).

Statistics

All data were evaluated for normal distribution with the Shapiro-Wilk test and are given as mean±SD. Statistical difference was assessed

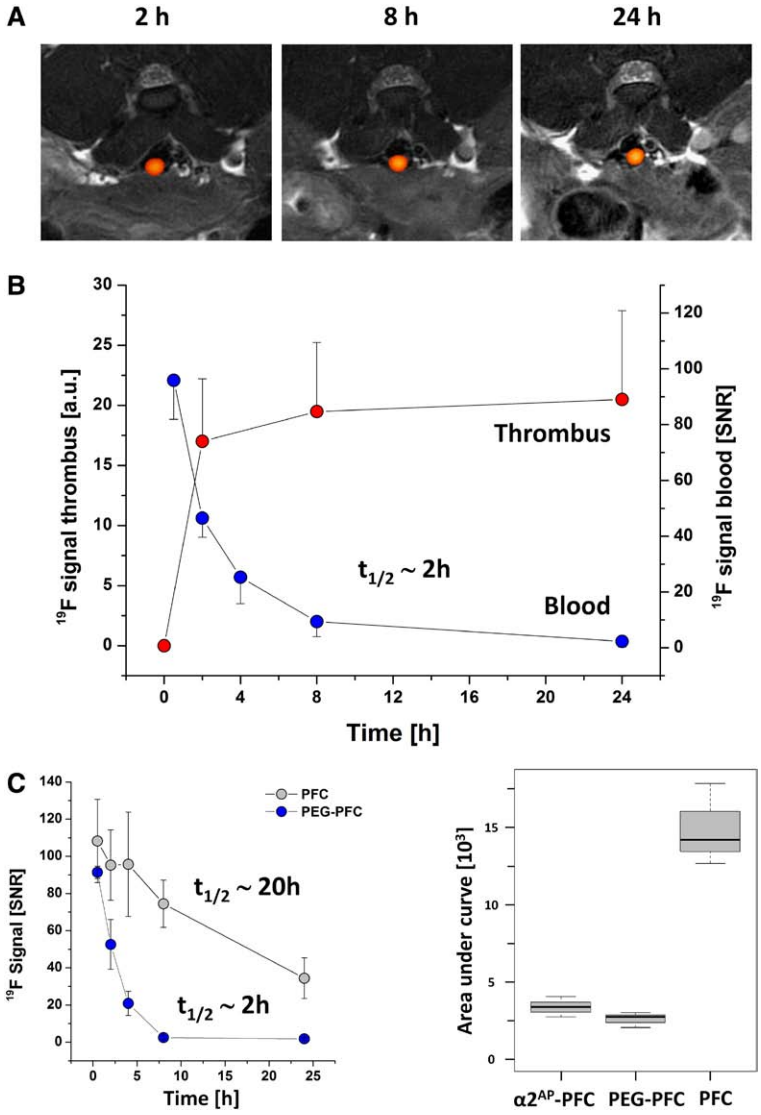

Figure 2. Time course of the ^{19}F signal in thrombi and blood. **A**, Sections of in vivo ^{1}H/^{19}F magnetic resonance imaging (MRI) scans of the same animal 2, 8, and 24 hours after thrombus induction. **B**, Kinetics of the total ^{19}F MR signal in venous thrombi (arbitrary units [a.u.], red circles) and ^{19}F signal in blood (signal-to-noise ratio [SNR], blue circles) after α2-antiplasmin peptide (α2^{AP})–perfluorocarbon nanoemulsion (PFC) injection determined by in vivo ^{19}F MRI. **C**, Time course of the blood signal (signal-to-noise ratio) after injection of PEGylated and unmodified PFCs determined by ^{19}F MRI (**left**). Area under the curve calculated from the blood ^{19}F signal over time (^{19}F signal·h) for α2^{AP}-PFCs, PEG-PFCs, and PFCs (**right**). **B** and **C**, Data represent mean±SD of n=3 experiments.

by the Welch test (for unequal variances), and a level of $P<0.05$ was considered statistically significant.

Results

Visualization of Deep Venous Thrombi by ^{1}H/^{19}F MRI In Vivo

To generate PFCs for the targeting of developing thrombi, we used a 14–amino acid peptide derived from α2^{AP} (Figure I in the online-only Data Supplement), which is cross-linked by FXIIIa to fibrin at the glutamine Q3 during the early phase of the thrombus development.[15–17] As control, we applied an FXIIIa low-affinity peptide in which glutamine was replaced by alanine in position 3 (Q3A).[15,16] Both peptides were coupled to cholesterol-PEG-maleimide and inserted into preformed PFCs by SPIT (Figure 1A).

To explore the suitability of α2^{AP}-PFCs for early thrombus detection, we induced nonocclusive thrombi in the inferior vena cava and injected α2^{AP}-PFCs or Q3A-PFCs intravenously 5 minutes before thrombus induction. After 2 hours, ^{1}H/^{19}F MRIs were acquired in the proximity of the thrombus induction site. As shown in Figure 1B, animals that received α2^{AP}-PFCs display a strong background-free ^{19}F signal at the site of the newly formed thrombus that can be dimly recognized in ^{1}H MRI at the ventral side of the vena cava as a dark gray structure (arrows in Figure 1B, bottom). Although α2^{AP}-PFCs clearly delineated the thrombus, no signal was found in the area surrounding the surgery (Figure 1B, top), indicating the specificity of labeling. ^{19}F signals were found to be substantially reduced when PFCs with Q3A–control peptide were used (Figure 1B, bottom). Quantification of all data revealed a strongly enhanced ^{19}F signal for α2^{AP}-PFCs compared with control Q3A-PFCs ($P<0.05$; Figure 1B, right). Note that the mean diameter of the thrombi was <1 mm (0.74±0.16 mm; n=8) and that mere angiographic MR ^{1}H scans did not permit us to precisely detect the location of the thrombus because only minor alterations in the blood flow were observed (Figure IIIA in the online-only Data Supplement). Although thrombi could be detected in high-resolution spin-echo MRIs, the calculated contrast-to-noise ratio for ^{1}H and ^{19}F signals between thrombus and the adjacent vessel lumen, muscle, and connective

tissue clearly revealed a strongly enhanced specificity of the ^{19}F hot spots with contrast-to-noise ratios increased at least 3-fold compared with ^{1}H images (Figure IIIB in the online-only Data Supplement).

To test whether the ^{19}F signal increases over time, we determined the time course of the ^{19}F signal 2, 8, and 24 hours after thrombus induction. From the representative magnifications of merged ^{1}H/^{19}F data sets (Figure 2A) and the quantitative analysis of all experiments (Figure 2B), it can be seen that there was no further PFC accumulation within the thrombus after 2 hours (Figure 2B, red circles). As expected, delayed application of the $\alpha2^{AP}$-PFCs after thrombus induction resulted in a continuous decline in the ^{19}F signal (Figure IVA in the online-only Data Supplement). In line with the reported half-life of FXIIIa activity of 20 to 30 minutes,[15–17] some ^{19}F signal could still be observed when $\alpha2^{AP}$-PFCs were injected 60 minutes after thrombus induction, whereas after 90 minutes, PFC deposition was not detected any longer. In separate in vivo experiments with untreated animals, we determined the ^{19}F signal in the blood by MRI (^{19}F FLASH) and found that the blood half-life of peptide-targeted PFCs was ≈2 hours (Figure 2B, blue circles). A similar half-life was found for PEGylated PFCs without peptide (Figure 2C, left), indicating that the PEGylation but not the peptide determines the kinetics within the circulation (Figure 2C, right). Interestingly, unmodified non-PEGylated PFCs remained in the bloodstream for a much longer time, with a half-life of ≈20 hours (Figure 2C).

To further corroborate the location of the ^{19}F signal within the thrombus, excised tissue samples were analyzed ex vivo by histology and by high-resolution ^{1}H/^{19}F MRI. Hematoxylin and eosin and Sirius Red staining confirmed thrombus formation, with the presence of trapped erythrocytes as a hallmark of deep venous thrombi (Figure 3A). Ex vivo MRI identified the thrombus as structure with inhomogeneous contrast surrounded by the dark vessel lumen and the embedding agarose (dark gray, Figure 3B; left, longitudinal sections; right, axial sections). Detected ^{19}F signal was clearly restricted to the thrombus and exhibited a patchy pattern distributed over the entire thrombus. This result was confirmed by histology through the use of PFCs with carboxyfluorescein-labeled $\alpha2^{AP}$-peptide, which also showed a patchy distribution of the fluorescence signal within the thrombus (Figure 3C, top). No signal could be observed in control thrombi from animals that received Q3A-carboxyfluorescein-PFCs (Figure 3C, bottom).

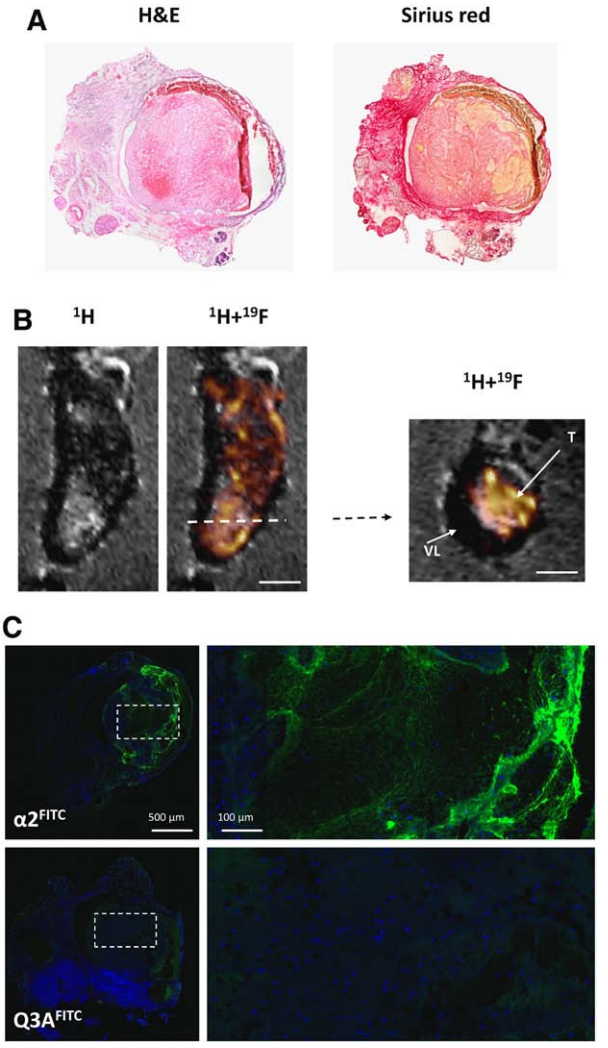

Figure 3. Ex vivo analysis of venous thrombi. **A**, Hematoxylin and eosin (H&E; **left**) and Sirius Red (**right**) staining of an thrombus induced by $FeCl_3$ in the inferior vena cava. **B**, High-resolution ^{1}H/^{19}F scan (0.5-nL voxel size) of an excised, paraformaldehyde-fixed, and agarose-embedded thrombus of the inferior vena cava. Longitudinal (**left**) and axial (**right**) sections are displayed showing ^{19}F signal (red) with patchy distribution over the entire thrombus. T indicates thrombus; and VL, vessel lumen. **C**, Histological analysis of thrombi after injection of carboxyfluorescein-labeled α2-antiplasmin peptide ($\alpha2^{AP}$)–perfluorocarbon nanoemulsions (PFCs; **top**). In control experiments, carboxyfluorescein-labeled Q3A-PFCs were applied (**bottom**). Nuclei are counterstained with DAPI. Scale bar represents 100/500 µm. The dashed lines indicate magnifications shown on the **right**. Note the appearance of the fibrin network in case of the $\alpha2^{AP}$ probe.

Specificity of $\alpha2^{AP}$-PFCs for Developing Thrombi

Trapping of PFC-loaded monocytes or PFCs themselves might have contributed to the observed ^{19}F signal in the thrombus. Therefore, we explored whether unmodified PFCs or PEGylated PFCs without peptide enrich in venous thrombi. As shown in Figure 4A, intravenous administration of PFCs or PEG-PFCs before thrombus induction did not lead to the deposition of any ^{19}F signal within thrombi (white arrows, Figure 4A). Flow cytometry on the cellular composition of thrombi revealed a small amount of CD45^{+}/CD11b^{+} immune cells (Figure 4B, left and middle) that consist predominantly of neutrophils and a negligible number of monocytes (Figure 4B, right). Interestingly, unmodified PFCs, which are known to be avidly taken up by macrophages,[22,23] gave rise to a strong ^{19}F signal in the inflamed area of surgery (Figure 4A, top, yellow arrows). In contrast, PEGylated PFCs did not accumulate in inflamed areas (Figure 4A, bottom). This phenomenon is most likely attributable to an impaired uptake of PEGylated PFCs by monocytes under these conditions. This assumption was confirmed by separate experiments, where the uptake of PEGylated PFCs by blood monocytes and RAW macrophages was found to be strongly reduced compared with neat

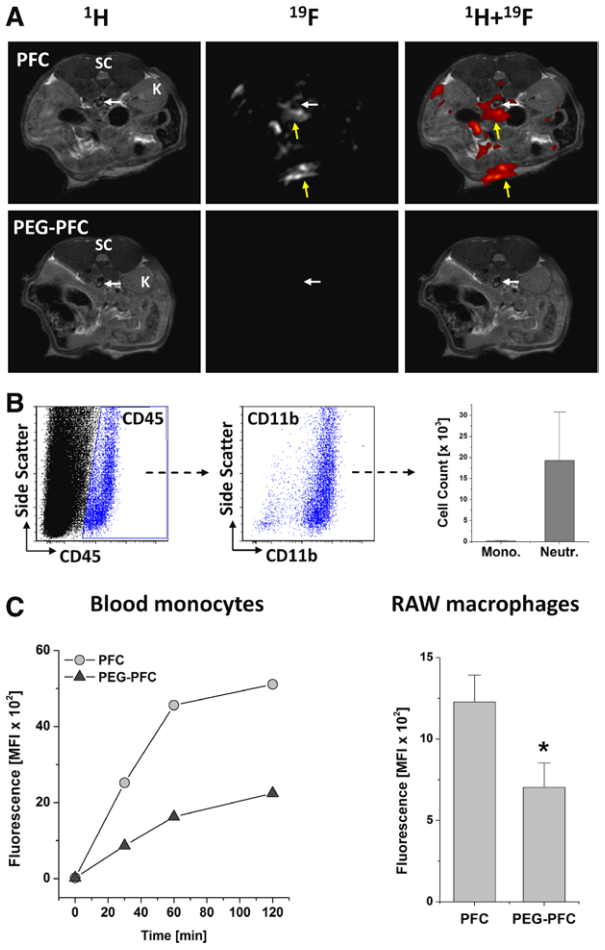

Figure 4. Nontargeted perfluorocarbon nanoemulsions (PFCs) do not accumulate in developing thrombi. **A**, In vivo $^{1}H/^{19}F$ magnetic resonance imaging of mice that received intravenously administered nontargeted PEGylated PFCs (PEG-PFC; **bottom**) or neat PFCs (PFCs; **top**) before thrombus induction. White arrows show the location of the thrombus; yellow arrows point to accumulation of neat PFCs in inflamed tissue resulting from surgical intervention for thrombus induction. Note the absence of any ^{19}F signal in the area of surgery for PEG-PFCs. **B**, Flow cytometric analysis of the cellular composition of venous thrombi showing that the small amount of thrombus-resident $CD45^{+}$ immune cells are predominantly $CD11b^{+}$ (**left** and **middle**). Further analyses revealed that this cell population is composed mainly of neutrophils and only a negligible amount of monocytes (**right**; data represent mean±SD of n=3 individual experiments). **C**, Decreased cellular uptake of PEGylated PFCs by blood monocytes (**left**) or RAW macrophages (**right**) determined by flow cytometry after incubation with rhodamine-labeled unmodified PFCs or rhodamine-labeled PEG-PFCs. RAW macrophages were incubated for 2 hours (n=9). **P*<0.05 vs neat PFCs.

PFCs (Figure 4C). Thus, neither PFC-loaded immune cells nor passive PFC accumulation contributed substantially to the $\alpha2^{AP}$-PFC–derived ^{19}F signal in $FeCl_3$-induced deep venous thrombi.

Detection of Pulmonary Thromboembolism

Venous thrombi are strongly prone to cause pulmonary thromboembolism. We therefore explored whether ^{19}F MRI is also suitable for the detection of thrombi accumulating in the lung. To this end, we injected human thrombin, known to elicit

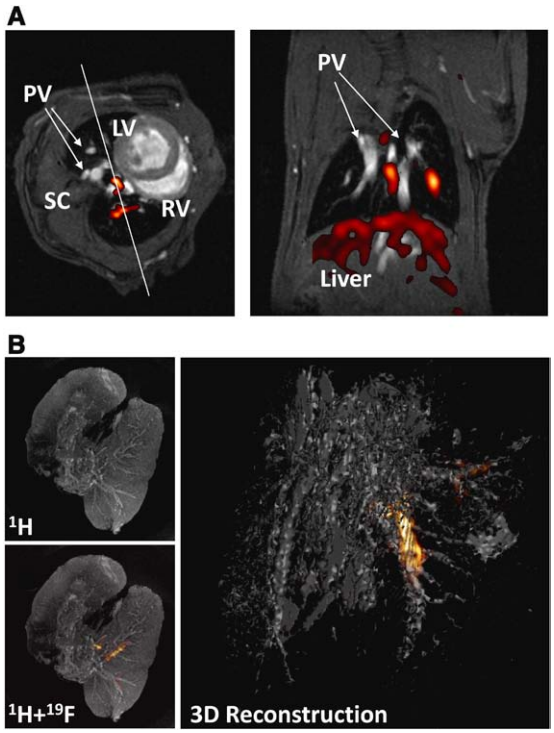

Figure 5. ^{19}F magnetic resonance imaging (MRI) of pulmonary embolism. **A**, Combined in vivo $^{1}H/^{19}F$ MRI of the mouse thorax showing strong ^{19}F signals within the lung after thrombin and $\alpha2$-antiplasmin peptide ($\alpha2^{AP}$)–perfluorocarbon nanoemulsion (PFC) injection. The white line within the axial image (**left**) indicates the location of the corresponding coronal slice shown on the **right**. LV indicates left ventricle; PV, pulmonary vessels; RV, right ventricle; and SC, spinal cord. **B**, Ex vivo postmortem high-resolution $^{1}H/^{19}F$ MRI of paraformaldehyde-fixed and agarose-embedded lung tissue indicating accumulation of ^{19}F signal next to the right pulmonary branch. The location of the ^{19}F signal (red) was further validated by 3-dimensional reconstruction of the data sets (**right**; Movie I in the online-only Data Supplement).

pulmonary thrombosis,[33] in combination with $\alpha2^{AP}$-PFCs. In vivo $^{1}H/^{19}F$ MR analyses of the thorax revealed strong ^{19}F signals in the lung (Figure 5A, left) that otherwise appear dark in conventional ^{1}H MRI scans because of the low proton density, with the exception of some signals arising from flowing blood in pulmonary vessels next to the heart (Figure 5A, arrows). The location of the ^{19}F signal in lung tissue of $\alpha2^{AP}$-PFC–treated animals was confirmed by coronal MR scans (Figure 5A, right). Note that ^{19}F signals can also be observed in the liver, which is known to be a major site of PFC accumulation.[34] The specificity of the ^{19}F signals was validated in separate experiments in which thrombin was injected in combination with untargeted PFCs or Q3A-PFCs. Under these conditions we found no ^{19}F signals in the lung (Figure V in the online-only Data Supplement). In addition, we performed ex vivo MR analyses and found ^{19}F signals in all animals that received thrombin plus $\alpha2^{AP}$-PFCs but not in control animals (thrombin plus neat PFCs; thrombin plus Q3A-PFCs). Figure 5B displays corresponding postmortem high-resolution MRI scans of the excised lung of the same animal shown in Figure 5A, which confirms the location of the ^{19}F signal within the right lobe of the lung (Figure 5B, left). Interestingly, 3-dimensional reconstruction of the data sets also revealed weaker signals

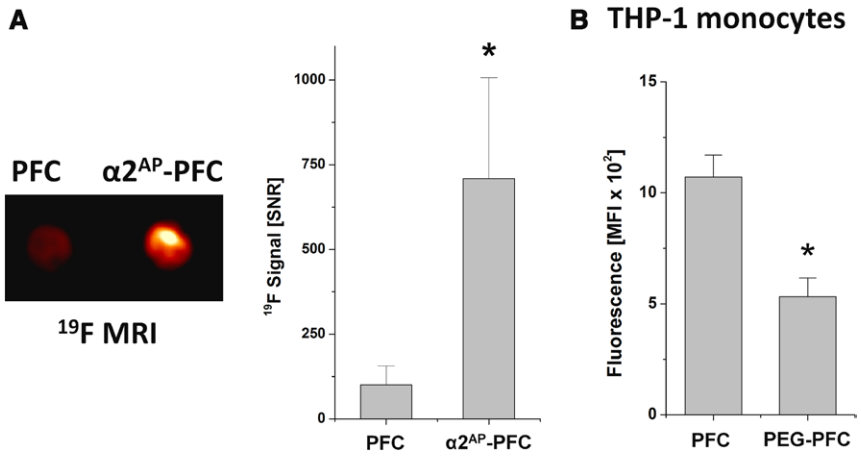

Figure 6. Labeling of human thrombi generated in vitro. **A**, Incorporation of nontargeted perfluorocarbon nanoemulsions (PFCs) or α2-antiplasmin peptide ($\alpha2^{AP}$)–PFCs into human thrombi generated in vitro. ^{19}F MR image (**left**) and quantified ^{19}F signal (**right**). **B**, Flow cytometric analysis of the uptake of PEGylated or unmodified PFCs by the human monocytic cell line THP-1. **A** and **B**, Data are mean±SD of n=10 experiments. *P<0.05 vs neat PFCs.

in the lung periphery (Figure 5B, right, and Movie I in the online-only Data Supplement).

Labeling of Human Thrombi With $\alpha2^{AP}$-PFCs

To test whether $\alpha2^{AP}$ bound to PFCs can also label human thrombi, human thrombi generated in vitro were treated with untargeted PFCs or $\alpha2^{AP}$-PFCs during the early phase of thrombus formation. As shown in Figure 6A, we observed a 10-fold-increased ^{19}F signal for $\alpha2^{AP}$-PFCs, indicating the specific incorporation of $\alpha2^{AP}$-PFCs. Of note, when $\alpha2^{AP}$-PFCs were applied after thrombus induction, similar time courses for the decline of the ^{19}F signal were obtained for human thrombi generated ex vivo and thrombi generated in vivo in the mouse (Figure IV in the online-only Data Supplement). Moreover, we found that the uptake of PEGylated PFCs compared with neat PFCs is likewise impaired for human THP-1 monocytes (Figure 6B).

Discussion

In the present study, we report a novel technique for the noninvasive detection of thrombi and pulmonary embolism that is based on ^{19}F MRI combined with $\alpha2^{AP}$-targeted PFCs. With the use of SPIT, targeting ligands were attached to preformed PFCs under mild conditions that maintained their integrity. This approach proved to be suitable for the detection of developing thrombi with a diameter of <1 mm in a reasonable scan time (30 minutes) and with high sensitivity (signal-to-noise ratio, 70). Specificity is further provided by the rapid clearance of $\alpha2^{AP}$-PFCs from the bloodstream by liver and spleen. In addition, uptake of $\alpha2^{AP}$-PFCs by blood monocytes is strongly impaired compared with unmodified PFCs, resulting in the absence of PFC accumulation in inflamed areas and therefore in a strongly reduced background signal.

Ultrasound is the gold standard for the diagnosis of deep venous thrombi of legs but is not suitable for structures located more deeply (eg, lung). ^{1}H MRI has a high spatial resolution, but the application of targeted contrast agents based on iron oxide may be difficult, particularly in lung tissue, which appears black in conventional MR scans. MR angiography can indicate the presence of thrombi, but the detection of small thrombi with only little impact on the blood flow is challenging. Consistent with this notion, we found no clear evidence for thrombus formation by ^{1}H-based MR angiography in the present study (Figure IIIA in the online-only Data Supplement). Unambiguous anatomic identification of thrombi by high-contrast ^{1}H spin-echo images, however, requires prior knowledge of the localization and a quite high resolution of the ^{1}H MRI. Similar considerations apply for the gadolinium-based contrast agent (EP-2104R) that has successfully been used for thrombus detection in a variety of preclinical animal studies and in humans.[6–11] In contrast, ^{19}F MRI, because of the lack of ^{19}F in the body, provides highly specific hot spots, and their anatomic location can be easily determined by merging with anatomic ^{1}H reference scans. This enabled us to precisely detect $\alpha2^{AP}$-PFC–labeled thrombi in the vena cava with high specificity and excellent signal-to-noise and contrast-to-noise ratios because of the low level of tissue background. Quantification of the ^{19}F signal within the thrombus revealed that 150 nmol ^{19}F nuclei per voxel (0.16 mm^3) resulted in a signal-to-noise ratio of ≈70 (Figure VI in the online-only Data Supplement). This translates to a local PFC concentration of ≈40 mmol/L, which is substantially higher than reported for EP-2104R (<0.25 mmol/L).[9,35–39] However, there are several future options to optimize our present approach: Enhanced sensitivity can be obtained by increased voxel size or by improvements in hardware and imaging sequences. Zhong et al[40] recently achieved an 8-fold decrease in scan time by implementing compressed sensing for ^{19}F MRI, which could alternatively be used for lowering the PFC doses. On the other hand, given the high signal-to-noise ratio observed in this study, the applied dose of the contrast agent could be reduced several-fold in either case.

Generation of targeted PFCs with labile ligands is generally hampered by the manufacturing process, which usually requires high pressure to obtain stable nanoemulsions with a narrow size distribution,[31] High-pressure homogenization causes substantial shear forces and cavitation; the latter generates local heat of up to 10^4 K by implosion of dispersant

gas bubbles resulting from low static pressure.[41] Obviously, such conditions are disadvantageous for the handling of sensitive ligands such as peptides, antibodies, or antibody fragments. This might explain the low signal-to-noise ratios of recent approaches for in vivo ^{19}F MRI using targeted PFCs in a tumor model and after lung ischemia.[42,43] SPIT, used here to modify preformed PFCs, overcomes the problem of possible ligand destruction when linked before high-pressure homogenization. Insertion of the targeting ligand by SPIT can be performed at room temperature with gentle agitation. Furthermore, SPIT-targeted PFCs can be produced in very small quantities down to ≤100 μL, which cannot be handled by conventional methods because homogenizers for such small volumes are not available. Importantly, this technique makes use of cholesterol-PEG, which is well tolerated by organism and cells (Figure IIC in the online-only Data Supplement). In addition, SPIT is not restricted to peptides and antibodies but also works with different reactive groups and ligands such as single-chain monoclonal antibodies or small proteins.

So far, ^{19}F MRI has been widely used for immune cell tracking because of the efficient uptake of unmodified PFCs by blood monocytes after intravenous injection.[21–25,27,29,32,34] Tracking of blood cells without phagocytic properties (such as T cells) or distinct cell types (dendritic cells, monocyte or macrophage subsets) previously required ex vivo labeling with PFCs and reimplantation.[44–46] However, attachment of specific ligands for distinct surface epitopes to PFCs by the postinsertion technique should enable the direct in vivo labeling of target cells after intravenous injection in future studies.

MRI offers excellent spatial resolution, and the sensitivity of $\alpha2^{AP}$-PFCs should be suitable to detect newly formed small thrombi that only partially affect the blood flow in thromboembolic lungs or deep veins in a clinically relevant situation. Specific assessment of early thrombus formation versus organized thrombi will improve the selection of patients who benefit from fibrinolytic therapy and will help to adequately adjust doses in lysis schemata, thereby reducing serious side effects such as bleeding in situations when chronic thrombi are resistant to fibrinolytic therapy. In vivo imaging of FXIIIa activity via $\alpha2^{AP}$-PFCs could further aid in monitoring of imminent thrombus formation after implantation of such devices as pacemakers, valves, or scaffolds and in identifying latent thrombus generation in structures characterized by low blood flow velocities and prone to stasis such as the left atrial appendage. Besides coupling α2-antiplasmin peptide, SPIT holds the potential to be adapted for single-chain monoclonal antibodies raised against activated glycoprotein IIb/IIIa[47] or peptides that bind to existing thrombi,[10] also enabling the assessment of persistent thrombi by ^{19}F MRI.

The method described here has significant translational potential. Similar to mice, $\alpha2^{AP}$-targeted PFCs also specifically bind to human thrombi (Figure 6) owing to the species-independent cross-linking of α2-antiplasmin with FXIIIa.[48] Specific targeting, in combination with PEGylation, also ensures that the nanoparticle uptake by monocytes is strongly reduced. Furthermore, perfluorocarbons are biochemically inert as a result of the strong C-F bond, which cannot be cleaved by enzymes, and are therefore nontoxic.[49] Human application of SPIT is feasible with the use of the clinically relevant perfluorooctyl bromide and perfluorodecalin emulsions, which are characterized by short biological half-lives[34] and have been used in human trials. Because of the excellent sensitivity and specificity, we propose that $\alpha2^{AP}$-PFCs, in conjunction with ^{19}F MRI, are a suitable future option for the detection of small thrombi even with a clinical MR scanner at 3 T.

Acknowledgments

We thank Bodo Steckel and Annika Zimmermann for excellent technical assistance, as well as Malte Kelm and Ralf Westenfeld for helpful discussions.

Sources of Funding

This work was supported by the Deutsche Forschungsgemeinschaft (DFG), subproject B2 of the Sonderforschungsbereich 1116, grant SCHR 154/13-2, and grant SCHU 800/8-2.

Disclosures

None.

References

1. Lauw MN, van Doormaal FF, Middeldorp S, Buller HR. Cancer and venous thrombosis: current comprehensions and future perspectives. *Semin Thromb Hemost*. 2013;39:507–514. doi: 10.1055/s-0033-1343891.
2. Stein PD, Beemath A, Olson RE. Obesity as a risk factor in venous thromboembolism. *Am J Med*. 2005;118:978–980. doi: 10.1016/j.amjmed.2005.03.012.
3. Baxter GM, McKechnie S, Duffy P. Colour Doppler ultrasound in deep venous thrombosis: a comparison with venography. *Clin Radiol*. 1990;42:32–36.
4. Thomas SM, Goodacre SW, Sampson FC, van Beek EJ. Diagnostic value of CT for deep vein thrombosis: results of a systematic review and meta-analysis. *Clin Radiol*. 2008;63:299–304. doi: 10.1016/j.crad.2007.09.010.
5. Sampson FC, Goodacre SW, Thomas SM, van Beek EJ. The accuracy of MRI in diagnosis of suspected deep vein thrombosis: systematic review and meta-analysis. *Eur Radiol*. 2007;17:175–181. doi: 10.1007/s00330-006-0178-5.
6. Andia ME, Saha P, Jenkins J, Modarai B, Wiethoff AJ, Phinikaridou A, Grover SP, Patel AS, Schaeffter T, Smith A, Botnar RM. Fibrin-targeted magnetic resonance imaging allows in vivo quantification of thrombus fibrin content and identifies thrombi amenable for thrombolysis. *Arterioscler Thromb Vasc Biol*. 2014;34:1193–1198. doi: 10.1161/ATVBAHA.113.302931.
7. Sirol M, Fuster V, Badimon JJ, Fallon JT, Moreno PR, Toussaint JF, Fayad ZA. Chronic thrombus detection with *in vivo* magnetic resonance imaging and a fibrin-targeted contrast agent. *Circulation*. 2005;112:1594–1600. doi: 10.1161/CIRCULATIONAHA.104.522110.
8. Sirol M, Aguinaldo JG, Graham PB, Weisskoff R, Lauffer R, Mizsei G, Chereshnev I, Fallon JT, Reis E, Fuster V, Toussaint JF, Fayad ZA. Fibrin-targeted contrast agent for improvement of in vivo acute thrombus detection with magnetic resonance imaging. *Atherosclerosis*. 2005;182:79–85. doi: 10.1016/j.atherosclerosis.2005.02.013.
9. Spuentrup E, Fausten B, Kinzel S, Wiethoff AJ, Botnar RM, Graham PB, Haller S, Katoh M, Parsons EC Jr, Manning WJ, Busch T, Günther RW, Buecker A. Molecular magnetic resonance imaging of atrial clots in a swine model. *Circulation*. 2005;112:396–399. doi: 10.1161/CIRCULATIONAHA.104.529941.
10. Spuentrup E, Botnar RM, Wiethoff AJ, Ibrahim T, Kelle S, Katoh M, Ozgun M, Nagel E, Vymazal J, Graham PB, Günther RW, Maintz D. MR imaging of thrombi using EP-2104R, a fibrin-specific contrast agent: initial results in patients. *Eur Radiol*. 2008;18:1995–2005. doi: 10.1007/s00330-008-0965-2.

11. Vymazal J, Spuentrup E, Cardenas-Molina G, Wiethoff AJ, Hartmann MG, Caravan P, Parsons EC Jr. Thrombus imaging with fibrin-specific gadolinium-based MR contrast agent EP-2104R: results of a phase II clinical study of feasibility. *Invest Radiol*. 2009;44:697–704. doi: 10.1097/RLI.0b013e3181b092a7.
12. Reed GL, Houng AK. The contribution of activated factor XIII to fibrinolytic resistance in experimental pulmonary embolism. *Circulation*. 1999;99:299–304.
13. Robinson BR, Houng AK, Reed GL. Catalytic life of activated factor XIII in thrombi: implications for fibrinolytic resistance and thrombus aging. *Circulation*. 2000;102:1151–1157.
14. Chen JW, Figueiredo JL, Wojtkiewicz GR, Siegel C, Iwamoto Y, Kim DE, Nolte MW, Dickneite G, Weissleder R, Nahrendorf M. Selective factor XIIa inhibition attenuates silent brain ischemia: application of molecular imaging targeting coagulation pathway. *JACC Cardiovasc Imaging*. 2012;5:1127–1138. doi: 10.1016/j.jcmg.2012.01.025.
15. Jaffer FA, Tung CH, Wykrzykowska JJ, Ho NH, Houng AK, Reed GL, Weissleder R. Molecular imaging of factor XIIIa activity in thrombosis using a novel, near-infrared fluorescent contrast agent that covalently links to thrombi. *Circulation*. 2004;110:170–176. doi: 10.1161/01.CIR.0000134484.11052.44.
16. Miserus RJ, Herías MV, Prinzen L, Lobbes MB, Van Suylen RJ, Dirksen A, Hackeng TM, Heemskerk JW, van Engelshoven JM, Daemen MJ, van Zandvoort MA, Heeneman S, Kooi ME. Molecular MRI of early thrombus formation using a bimodal alpha2-antiplasmin-based contrast agent. *JACC Cardiovasc Imaging*. 2009;2:987–996. doi: 10.1016/j.jcmg.2009.03.015.
17. Tung CH, Ho NH, Zeng Q, Tang Y, Jaffer FA, Reed GL, Weissleder R. Novel factor XIII probes for blood coagulation imaging. *Chembiochem*. 2003;4:897–899. doi: 10.1002/cbic.200300602.
18. Ahrens ET, Bulte JW. Tracking immune cells in vivo using magnetic resonance imaging. *Nat Rev Immunol*. 2013;13:755–763. doi: 10.1038/nri3531.
19. Stoll G, Basse-Lüsebrink T, Weise G, Jakob P. Visualization of inflammation using (19) F-magnetic resonance imaging and perfluorocarbons. *Wiley Interdiscip Rev Nanomed Nanobiotechnol*. 2012;4:438–447. doi: 10.1002/wnan.1168.
20. Temme S, Bönner F, Schrader J, Flögel U. ^{19}F magnetic resonance imaging of endogenous macrophages in inflammation. *Wiley Interdiscip Rev Nanomed Nanobiotechnol*. 2012;4:329–343. doi: 10.1002/wnan.1163.
21. Balducci A, Wen Y, Zhang Y, Helfer BM, Hitchens TK, Meng WS, Wesa AK, Janjic JM. A novel probe for the non-invasive detection of tumor-associated inflammation. *Oncoimmunology*. 2013;2:e23034. doi: 10.4161/onci.23034.
22. Ebner B, Behm P, Jacoby C, Burghoff S, French BA, Schrader J, Flögel U. Early assessment of pulmonary inflammation by ^{19}F MRI in vivo. *Circ Cardiovasc Imaging*. 2010;3:202–210. doi: 10.1161/CIRCIMAGING.109.902312.
23. Flögel U, Ding Z, Hardung H, Jander S, Reichmann G, Jacoby C, Schubert R, Schrader J. In vivo monitoring of inflammation after cardiac and cerebral ischemia by fluorine magnetic resonance imaging. *Circulation*. 2008;118:140–148. doi: 10.1161/CIRCULATIONAHA.107.737890.
24. Flögel U, Su S, Kreideweiss I, Ding Z, Galbarz L, Fu J, Jacoby C, Witzke O, Schrader J. Noninvasive detection of graft rejection by in vivo (19) F MRI in the early stage. *Am J Transplant*. 2011;11:235–244. doi: 10.1111/j.1600-6143.2010.03372.x.
25. Flögel U, Burghoff S, van Lent PL, Temme S, Galbarz L, Ding Z, El-Tayeb A, Huels S, Bönner F, Borg N, Jacoby C, Müller CE, van den Berg WB, Schrader J. Selective activation of adenosine A2A receptors on immune cells by a CD73-dependent prodrug suppresses joint inflammation in experimental rheumatoid arthritis. *Sci Transl Med*. 2012;4:146ra108. doi: 10.1126/scitranslmed.3003717.
26. Hertlein T, Sturm V, Kircher S, Basse-Lüsebrink T, Haddad D, Ohlsen K, Jakob P. Visualization of abscess formation in a murine thigh infection model of *Staphylococcus aureus* by ^{19}F-magnetic resonance imaging (MRI). *PLoS One*. 2011;6:e18246. doi: 10.1371/journal.pone.0018246.
27. Jacoby C, Borg N, Heusch P, Sauter M, Bönner F, Kandolf R, Klingel K, Schrader J, Flögel U. Visualization of immune cell infiltration in experimental viral myocarditis by (19)F MRI in vivo. *MAGMA*. 2014;27:101–106. doi: 10.1007/s10334-013-0391-6.
28. Weise G, Basse-Lüsebrink TC, Kleinschnitz C, Kampf T, Jakob PM, Stoll G. In vivo imaging of stepwise vessel occlusion in cerebral photothrombosis of mice by 19F MRI. *PLoS One*. 2011;6:e28143. doi: 10.1371/journal.pone.0028143.
29. Weise G, Basse-Luesebrink TC, Wessig C, Jakob PM, Stoll G. In vivo imaging of inflammation in the peripheral nervous system by (19)F MRI. *Exp Neurol*. 2011;229:494–501. doi: 10.1016/j.expneurol.2011.03.020.
30. Manjappa AS, Chaudhari KR, Venkataraju MP, Dantuluri P, Nanda B, Sidda C, Sawant KK, Murthy RS. Antibody derivatization and conjugation strategies: application in preparation of stealth immunoliposome to target chemotherapeutics to tumor. *J Control Release*. 2011;150:2–22. doi: 10.1016/j.jconrel.2010.11.002.
31. Mayenfels F. *Fluorcarbonhaltige Nanoemulsionen zur Anwendung in der ^{1}H/^{19}F-Magnetresonanztomographie* Albert-Ludwigs Universität, Freiburg i. Br.; Thesis, 2012.
32. Temme S, Jacoby C, Ding Z, Bönner F, Borg N, Schrader J, Flögel U. Technical advance: monitoring the trafficking of neutrophil granulocytes and monocytes during the course of tissue inflammation by noninvasive ^{19}F MRI. *J Leukoc Biol*. 2014;95:689–697. doi: 10.1189/jlb.0113032.
33. Gresele P, Momi S, Berrettini M, Nenci GG, Schwarz HP, Semeraro N, Colucci M. Activated human protein C prevents thrombin-induced thromboembolism in mice: evidence that activated protein C reduces intravascular fibrin accumulation through the inhibition of additional thrombin generation. *J Clin Invest*. 1998;101:667–676. doi: 10.1172/JCI575.
34. Jacoby C, Temme S, Mayenfels F, Benoit N, Krafft MP, Schubert R, Schrader J, Flögel U. Probing different perfluorocarbons for in vivo inflammation imaging by ^{19}F MRI: image reconstruction, biological half-lives and sensitivity. *NMR Biomed*. 2014;27:261–271. doi: 10.1002/nbm.3059.
35. Spuentrup E, Katoh M, Wiethoff AJ, Parsons EC Jr, Botnar RM, Mahnken AH, Günther RW, Buecker A. Molecular magnetic resonance imaging of pulmonary emboli with a fibrin-specific contrast agent. *Am J Respir Crit Care Med*. 2005;172:494–500. doi: 10.1164/rccm.200503-379OC.
36. Spuentrup E, Buecker A, Katoh M, Wiethoff AJ, Parsons EC Jr, Botnar RM, Weisskoff RM, Graham PB, Manning WJ, Günther RW. Molecular magnetic resonance imaging of coronary thrombosis and pulmonary emboli with a novel fibrin-targeted contrast agent. *Circulation*. 2005;111:1377–1382. doi: 10.1161/01.CIR.0000158478.29668.9B.
37. Spuentrup E, Katoh M, Wiethoff AJ, Parsons EC Jr, Botnar RM, Mahnken AH, Günther RW, Buecker A. Molecular magnetic resonance imaging of pulmonary emboli with a fibrin-specific contrast agent. *Am J Respir Crit Care Med*. 2005;172:494–500. doi: 10.1164/rccm.200503-379OC.
38. Spuentrup E, Katoh M, Buecker A, Fausten B, Wiethoff AJ, Wildberger JE, Haage P, Parsons EC Jr, Botnar RM, Graham PB, Vettelschoss M, Günther RW. Molecular MR imaging of human thrombi in a swine model of pulmonary embolism using a fibrin-specific contrast agent. *Invest Radiol*. 2007;42:586–595. doi: 10.1097/RLI.0b013e31804fa154.
39. Spuentrup E, Katoh M, Wiethoff AJ, Buecker A, Botnar RM, Parsons EC, Guenther RW. Molecular coronary MR imaging of human thrombi using EP-2104R, a fibrin-targeted contrast agent: experimental study in a swine model. *Rofo*. 2007;179:1166–1173. doi: 10.1055/s-2007-963573.
40. Zhong J, Mills PH, Hitchens TK, Ahrens ET. Accelerated fluorine-19 MRI cell tracking using compressed sensing. *Magn Reson Med*. 2013;69:1683–1690. doi: 10.1002/mrm.24414.
41. Brandl M. *Verkapselung von gereinigtem Hämoglobin in Liposomen nach einem neuen und effizienten Verfahren.* Albert-Ludwigs Universität, Freiburg i. Br.; Thesis, 1990..
42. Giraudeau C, Geffroy F, Mériaux S, Boumezbeur F, Robert P, Port M, Robic C, Le Bihan D, Lethimonnier F, Valette J. ^{19}F molecular MR imaging for detection of brain tumor angiogenesis: in vivo validation using targeted PFOB nanoparticles. *Angiogenesis*. 2013;16:171–179. doi: 10.1007/s10456-012-9310-0.
43. Schmieder AH, Wang K, Zhang H, Senpan A, Pan D, Keupp J, Caruthers SD, Wickline SA, Shen B, Wagner EM, Lanza GM. Characterization of early neovascular response to acute lung ischemia using simultaneous (19)F/ (1)H MR molecular imaging. *Angiogenesis*. 2014;17:51–60. doi: 10.1007/s10456-013-9377-2.
44. Ahrens ET, Flores R, Xu H, Morel PA. In vivo imaging platform for tracking immunotherapeutic cells. *Nat Biotechnol*. 2005;23:983–987. doi: 10.1038/nbt1121.
45. Srinivas M, Morel PA, Ernst LA, Laidlaw DH, Ahrens ET. Fluorine-19 MRI for visualization and quantification of cell migration in a diabetes model. *Magn Reson Med*. 2007;58:725–734. doi: 10.1002/mrm.21352.
46. Srinivas M, Turner MS, Janjic JM, Morel PA, Laidlaw DH, Ahrens ET. In vivo cytometry of antigen-specific T cells using ^{19}F MRI. *Magn Reson Med*. 2009;62:747–753. doi: 10.1002/mrm.22063.

47. Wang X, Hagemeyer CE, Hohmann JD, Leitner E, Armstrong PC, Jia F, Olschewski M, Needles A, Peter K, Ahrens I. Novel single-chain antibody-targeted microbubbles for molecular ultrasound imaging of thrombosis: validation of a unique noninvasive method for rapid and sensitive detection of thrombi and monitoring of success or failure of thrombolysis in mice. *Circulation*. 2012;125:3117–3126. doi: 10.1161/CIRCULATIONAHA.111.030312.
48. Arnout J. *Thrombosis: Fundamental and Clinical Aspects*. Leuven, Belgium: Leuven University Press; 2003.
49. Wolters M, Mohades SG, Hackeng TM, Post MJ, Kooi ME, Backes WH. Clinical perspectives of hybrid proton-fluorine magnetic resonance imaging and spectroscopy. *Invest Radiol*. 2013;48:341–350. doi: 10.1097/RLI.0b013e318277528c.

CLINICAL PERSPECTIVE

The formation of fibrin-rich deep venous thrombi has a high incidence in the elderly, obese people, and, especially, in patients with tumors, strongly affecting morbidity and mortality. For specific visualization of newly formed thrombi, we used α2-antiplasmin peptide–labeled perfluorocarbon nanoemulsions as the contrast agent, which is cross-linked by factor XIIIa to the developing fibrin network. By simultaneous acquisition of matching anatomic proton (^{1}H) and fluorine (^{19}F) magnetic resonance images, this approach can precisely locate newly formed thrombi as "hot spots." ^{19}F magnetic resonance imaging is a background-free imaging approach that provides robust signals with an excellent degree of specificity, allowing an imaging scenario in the clinical setting as follows: Without prior knowledge of the thrombus location, a fast, low-resolution, whole-body ^{19}F magnetic resonance imaging scan could be carried out. After identification of 1 or more ^{19}F hot spots, additional high-resolution ^{1}H and ^{19}F scans could be recorded solely at these predefined regions for unambiguous anatomic localization of the developed thrombi. The specific assessment of early thrombus formation versus organized thrombi can improve the selection of patients who benefit from fibrinolytic therapy and help to adjust doses in lysis schemata, reducing serious side effects when chronic thrombi are resistant to therapy. In vivo imaging of factor XIIIa activity via α2-antiplasmin peptide–labeled perfluorocarbon nanoemulsions could further aid in monitoring of imminent thrombus formation after implantation of devices such as pacemakers, valves, or scaffolds and in identifying latent thrombus generation in structures characterized by low blood flow velocities and prone to stasis such as the left atrial appendage.